ChemPubSoc Europe

DOI: 10.1002/chem.201703244

CHEMISTRY A European Journal Full Paper

Drug Design

Conformational Aspects in the Design of Inhibitors for Serine Hydroxymethyltransferase (SHMT): Biphenyl, Aryl Sulfonamide, and Aryl Sulfone Motifs

Geoffrey Schwertz,[a] Michelle S. Frei,[a] Matthias C. Witschel,[b] Matthias Rottmann,[c, d] Ubolsree Leartsakulpanich,[e] Penchit Chitnumsub,[e] Aritsara Jaruwat,[e] Wanwipa Ittarat,[e] Anja Schäfer,[c, d] Raphael A. Aponte,[b] Nils Trapp,[a] Kerstin Mark,[a] Pimchai Chaiyen,[f, g] and François Diederich*[a]

Abstract: Malaria remains a major threat to mankind due to the perpetual emergence of resistance against marketed drugs. Twenty-one pyrazolopyran-based inhibitors bearing terminal biphenyl, aryl sulfonamide, or aryl sulfone motifs were synthesized and tested towards serine hydroxymethyltransferase (SHMT), a key enzyme of the folate cycle. The best ligands inhibited *Plasmodium falciparum* (*Pf*) and *Arabidopsis thaliana* (*At*) SHMT in target, as well as *Pf*NF54 strains in cell-based assays in the low nanomolar range (18–56 nM). Seven co-crystal structures with *P. vivax* (*Pv*) SHMT were solved at 2.2–2.6 Å resolution. We observed an unprecedented influence of the torsion angle of *ortho*-substituted biphenyl moieties on cell-based efficacy. The peculiar lipophilic character of the sulfonyl moiety was highlighted in the complexes with aryl sulfonamide analogues, which bind in their preferred staggered orientation. The results are discussed within the context of conformational preferences in the ligands.

[a] *G. Schwertz, M. S. Frei, Dr. N. Trapp, K. Mark, Prof. Dr. F. Diederich*
Laboratorium für Organische Chemie, ETH Zurich
Vladimir-Prelog-Weg 3, 8093 Zurich (Switzerland)
E-mail: diederich@org.chem.ethz.ch

[b] *Dr. M. C. Witschel, Dr. R. A. Aponte*
BASF SE, Carl-Bosch-Strasse 38, 67056 Ludwigshafen (Germany)

[c] *Dr. M. Rottmann, A. Schäfer*
Swiss Tropical and Public Health Institute (SwissTPHI)
Socinstrasse 57, 4051 Basel (Switzerland)

[d] *Dr. M. Rottmann, A. Schäfer*
Universität Basel, Petersplatz 1, 4003 Basel (Switzerland)

[e] *Dr. U. Leartsakulpanich, Dr. P. Chitnumsub, A. Jaruwat, W. Ittarat*
National Center for Genetic Engineering and Biotechnology
113 Thailand Science Park, Phahonyothin Road
Pathumthani 12120 (Thailand)

[f] *Prof. Dr. P. Chaiyen*
Department of Biochemistry and Center for Excellence in Protein and Enzyme Technology, Faculty of Science Mahidol University
272 Rama VI Road, Bangkok 10400 (Thailand)

[g] *Prof. Dr. P. Chaiyen*
Department of Biomolecular Science and Engineering
School of Biomolecular Science & Engineering
Vidyasirimedhi Institute of Science and Technology (VISTEC)
Wangchan Valley, Rayong 21210 (Thailand)

Supporting information and the ORCID identification number(s) for the author(s) of this article can be found under: https://doi.org/10.1002/chem.201703244. It contains all synthetic procedures, characterizations of all new compounds, and their $^{1}H/^{13}C/^{19}F$ NMR spectra; detailed biological activities; additional data from the CSD and PDB searches; theoretical calculations; additional figures on protein-ligand interactions and design of ligands by modeling; and small-molecule crystal structures data. The coordinates files of the PvSHMT-ligand complexes were deposited in the PDB with the following access codes: 5XMP, 5XMQ, 5XMR, 5XMS, 5XMT, 5XMU, and 5XMV.

Introduction

Medicinal chemists enjoy diverse computational tools to support their drug development efforts, going from pK_a or log*D* calculations to more sophisticated predictions of preferential ligand docking modes by molecular modeling or protein–ligand binding energies by free energy calculations.[1–3] Docking and modeling of protein–ligand interactions have become a common routine to prioritize ideas for synthesis. The gain in Gibbs protein–ligand binding energy becomes enhanced with increasing degree of preorganization of the ligand; in other words, the preferred conformations of bound and unbound ligands should be similar.[4,5] A difference in conformational energy between free and bound state of $\Delta\Delta G_{\text{unbound}\rightarrow\text{bound}} \approx 1.4\ \text{kcal mol}^{-1}$ already translates into a tenfold decrease in Gibbs binding energy.[6,7] Some reports suggest to set the threshold for the bioactive conformation at 3 kcal mol^{-1} of the lowest energy conformation,[6,8] whereas others give a maximum Gibbs energy difference of 5 kcal mol^{-1}.[1,9] While the energetics of the conformations of free and bound ligand can be evaluated by computational methods,[5,10] conformational preferences of small molecules are best extracted from searches in the Cambridge Structural Database (CSD),[11–14] reaching more than 875 000 entries in 2017.[15,16] The potential of conformational searches in the CSD was nicely illustrated by Brameld et al.,[7] who reported a comprehensive study on most of the structural motifs used in medicinal chemistry. Recently Cottrell et al. expanded this CSD search to various ring fragments.[17]

Herein, we report two new series of ligands based on a pyrazolopyran core that inhibit the enzyme serine hydroxymethyltransferase (SHMT) and analyze how their molecular conformations profoundly affect binding geometry and biological activity. This enzyme is a crucial component of the folate synthesis cycle,[18,19] which is an essential pathway for the replication of *Plasmodium* parasites causing malaria. SHMT is a pyridoxal 5′-phosphate (PLP)-dependent enzyme catalyzing the one-carbon-unit transfer from serine to tetrahydrofolate (H_4F) (Figure 1).[20–24] We previously reported pyrazolopyran-based ligands as the first inhibitors of *Plasmodium falciparum* (*Pf*) SHMT with both target affinities IC_{50} (half maximal inhibitory concentration) and high in vitro efficacy EC_{50} (half maximal effective concentration) against the *P. falciparum* strain NF54 in the low nanomolar range, as illustrated for (±)-**1** (Figure 1c).[25]

Lately, we showed that optimized inhibitors targeting SHMT induce a significant reduction of parasitemia in vivo in a mouse model.[26] In this optimization program, we also investigated a series of seven ligands bearing an *ortho*-substituted terminal phenyl ring, replacing the thiophene ring in (±)-**1**. We report here the influence of the nature of the *ortho*-substituent on biological activity. The torsion angles of *ortho*-substituted biphenyl motifs were investigated in CSD and Protein Data Bank (PDB)[27,28] searches, as well as by a computational study, in order to understand the observed conformational effects.[29–31] We show that the torsion angle of the biphenyl fragment does not affect target affinity much, but rather influences cell-based efficacy with a steep structure–activity relationship (SAR), presumably by impacting cell-penetration and/or transporter-mediated uptake and efflux. In parallel, a second series of fourteen ligands, incorporating aryl sulfonamide or aryl sulfone moieties, was prepared and studied. We aimed at improving binding affinities to *Pf*SHMT by taking advantage of the distinct conformational preferences of these fragments[7,32–41] to establish interactions of lipophilic substituents on the ligand with the hydrophobic residues lining the channel (Figure 1c), which hosts the *para*-aminobenzoate (*p*ABA) side chain of the natural substrate H_4F. However, no significant gain in inhibitory activity could be measured with those extended ligands. From new co-crystal structures with *Plasmodium vivax* (*Pv*) SHMT, we document the profound preference of the sulfonyl moiety in the ligands to bind into hydrophobic, rather than hydrophilic environments, thereby exposing the hydrophobic substituents to solvent. Seven new co-crystal structures, paired with small-molecule X-ray crystallography, also enabled a comparison between the conformations of the bound and unbound biphenyl, aryl sulfonamide, and aryl sulfone ligands.

Results and Discussion

Ligand design

Molecular modeling with MOLOC,[42] using the two previously obtained co-crystal structures with pyrazolopyran-based inhibitors,[25] guided the structural modifications of the ligands. A schematic representation of the binding mode of (+)-**1** at the active site of *Pv*SHMT (PDB ID code: 4TMR) is depicted in Figure 1c. Two sub-pockets are conspicuous: the pyrazolopyran core binds into the pteridine binding pocket, which normally hosts the pteridine core of H_4F (PDB ID code: 4OYT).[24] The second sub-pocket is the *p*ABA channel, which is occupied by the *p*ABA side chain of H_4F. We designed two new series of ligands to establish improved interactions with the hydrophobic amino acid residues lining this channel. The pyrazolopyran core and its alkyl substituents (methyl and isopropyl) were kept intact. The CN moiety of (+)-**1** on the phenyl ring depart-

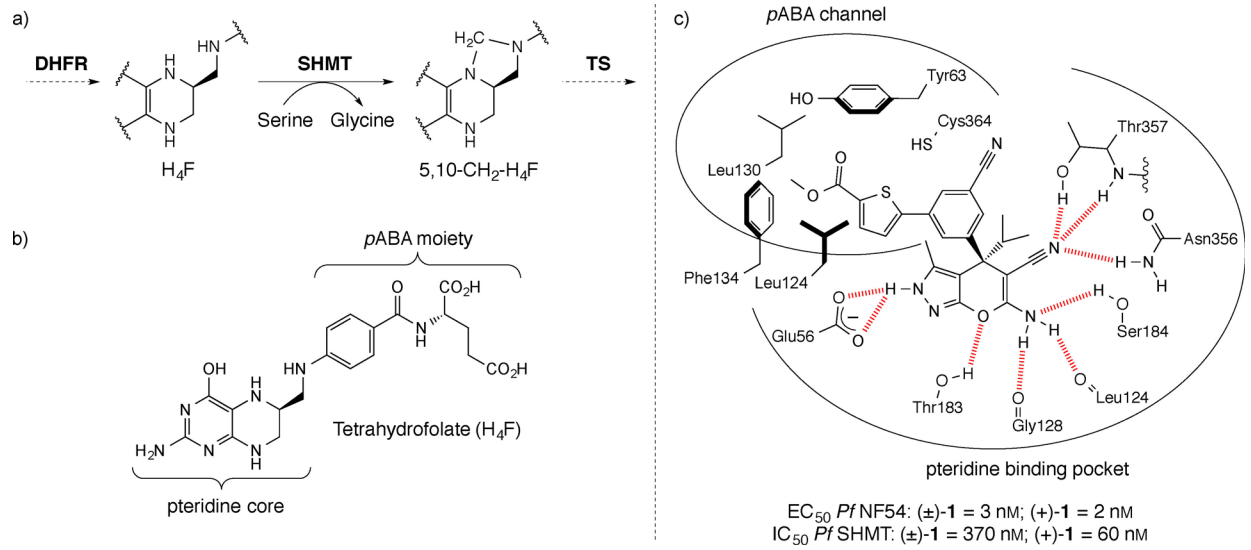

Figure 1. a) The one-carbon-unit transfer reaction catalyzed by SHMT. Dihydrofolate reductase (DHFR), SHMT, and thymidylate synthase (TS) are the three enzymes involved in the folate cycle. SHMT converts H_4F to 5,10-methylenetetrahydrofolate (5,10-CH_2-H_4F), a crucial component for the conversion of deoxyuridine monophosphate (dUMP) to the DNA precursor deoxythymidine monophosphate (dTMP) by TS. b) Molecular structure of H_4F. c) Schematic depiction of the binding mode of the initial lead (+)-**1** as seen in a co-crystal structure analysis (PDB ID code: 4TMR).[25] Intermolecular hydrogen bonding is indicated by red dashed lines.

ing from this core was exchanged for a CF_3 substituent, which was found to considerably improve ligand potency.[26] All other modifications are reported in the following.

Synthesis

The same synthetic pathway[25,26] was followed to prepare all pyrazolopyran-based ligands ((±)-**2**–**22**) reported in this manuscript (Scheme 1; for the full structures of all ligands, see Tables 1 and 2 below). Brominated **23** was either converted into the pinacol boronate ester **24** prior to a Suzuki cross-coupling[43] (for (±)-**2**–**20**) or directly subjected to a Buchwald–Hartwig cross-coupling[44] (for (±)-**21** and (±)-**22**) leading to intermediates **25a**–**u**. A subsequent Knoevenagel condensation[45] gave access to the dinitrile precursors **26a**–**u** needed for the one-pot synthesis of the pyrazolopyran core involving a Michael addition of 3-methyl-1*H*-pyrazol-5(4*H*)-one, followed by an intramolecular cyclization to provide (±)-**2**–**22** (for details, see the Supporting Information, Section S1).

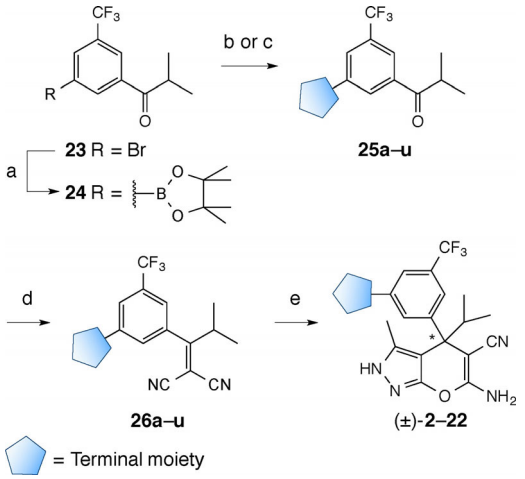

Scheme 1. Representative synthesis of pyrazolopyran-based ligands (±)-**2**–**22**. Reagents and conditions: a) bis(pinacolato)diboron, KOAc, $[PdCl_2(dppf)]\cdot CH_2Cl_2$ (2.0 mol%), toluene, μw, 150 °C, 6 min, 99%; b) **23** and corresponding aryl boronic acid or **24** and bromoaryl analogue, $[PdCl_2(PPh_3)_2]$ (5.0 mol%), Na_2CO_3, THF/H_2O 4:1, 60 °C, 4–16 h; c) **23**, corresponding amine, Cs_2CO_3, $[Pd_2(dba)_3]$ (2.0 mol%), X-Phos (8.0 mol%), 1,4-dioxane, 110 °C, 16 h; d) malononitrile, $TiCl_4$, pyridine, $CHCl_3$, 63 °C, 48–72 h; e) 3-methyl-1*H*-pyrazol-5(4*H*)-one, piperidine, 1,4-dioxane/EtOH 1:1, μw, 65 °C, 3.5 h. dba = dibenzylideneacetone; dppf = 1,1′-bis(diphenylphosphino)ferrocene; THF = tetrahydrofuran; X-Phos = 2-dicyclohexylphosphino-2′,4′,6′-triisopropylbiphenyl; μw = microwave irradiaton.

Biphenyl series

Biphenyl is the most common motif found in small-molecule drugs, therefore, it is important to understand its preferred conformation depending on its substitution pattern.[7] The geometry of a biphenyl motif can be tuned depending on intramolecular interactions. Modification of the substitution pattern often aims at improving protein–ligand interactions by orienting the two rings and the attached exit vectors in a precise way. Incorporation of heteroatoms can also strongly influence the overall conformation, for instance by sulfur/lone-pair interaction (chalcogen bonding) as reported recently.[9]

ortho-Substituted biphenyl analogues (±)-**2**–**8** (Table 1) were at first prepared to improve the intermolecular interactions with hydrophobic residues within the *p*ABA channel, such as Tyr63, Leu124, Leu130, and Phe134 (Figure 1c). For instance, modeling of (±)-**8** suggested the establishment of several favorable contacts with these four residues and additionally with Phe266 and Pro267 (Supporting Information, Section S5, Figure S12). Nevertheless, the unsubstituted analogue (±)-**2** was the most active ligand of the series in the target assay against *Pf*SHMT ($IC_{50} = 111 \pm 5$ nM, Table 1) and introduction of larger substituents led to weaker binding. IC_{50} values were also measured against *Arabidopsis thaliana* (*At*) SHMT to refine the SAR, as the plant enzyme and *Pf*SHMT are highly similar with 45% of sequence identity.[26,46] Stronger inhibition was obtained on *At*SHMT with IC_{50} values ranging from 7.3 to 32.0 nM (Table 1). Overall, a rather flat SAR was revealed in both target-based assays. In contrast, the nature of the *ortho*-substituent exerted a significant influence on the cell-based potency (EC_{50}) and a steep SAR was obtained. Increase in size of the *ortho*-substituent led to considerable decrease in antiparasitic efficacy from $EC_{50} = 18$ nM ((±)-**2**) to 665 nM ((±)-**8**) (Table 1). No direct correlation between cellular potency and lipophilicity (*clogP*) is distinguishable.

To explain these observations, we examined the torsion angles (τ) of biphenyl motifs in the CSD and the PDB.[47] An increase in size of an *ortho*-substituent directly translates into a larger torsion angle between the two ring planes (Table 1), similarly to the report by Brameld et al.[7] (Figure 2). However, it is essential to keep in mind that differences may occur between the solid and solution phase and that unsubstituted biphenyl is especially susceptible to crystal packing effects.[48] For instance, the torsion angle for biphenyl without any substituent is located around 35° (Figure 2a) and is slightly lower than the average torsion angle in the gas phase of 44°.[48] By introducing any substituent, the torsion angle shifts to higher values located above 50° (Figure 2b and Supporting Information, Section S3, Figure S1). A small-molecule X-ray crystal structure recorded for (±)-**6** displayed a torsion angle of 57.5°, which is nearly identical to the median value found in the CSD search (Supporting Information, Section S6.2.1, Figure S24). Not surprisingly, the *ortho*-CF_3 biphenyl possesses the highest torsion angle, although some caution is advised as only 6 structures were found in the CSD (Table 1 and Supporting Information, Section S3, Figure S1).

Next, a potential energy scan (PES) at the B3LYP/cc-pVDZ level of theory (in water with polarizable continuum solvent model) using Gaussian 09[49] was performed for each compound by incremental rotation of the terminal ring around the biphenyl axis (Supporting Information, Section S4, Figures S8 and S9). The most favorable biphenyl torsion angles calculated for all compounds (±)-**2**–**8** range from 36.5° to 62.0°, in agreement with the CSD search results. Additionally, the energy gap between the least stable, co-planar geometry and the most stable conformations increases with the size of the *ortho*-substituent. For example, for (±)-**2** without an *ortho*-substitu-

Table 1. Biological activities of biphenyl analogues (±)-**2**–**8**.

Cpd.	R	EC_{50} *Pf*NF54 [nM]	IC_{50} *Pf*SHMT ± SD [nM][a]	IC_{50} *At*SHMT [nM]	Biphenyl Median τ [°][b]	clog*P*[c]
(±)-**2**	H	18	111 ± 5	18.6	30.3	5.2
(±)-**3**	F	20	144 ± 0	7.3	43.2	4.9
(±)-**4**	Me	27	263 ± 11	30.9	55.5	5.3
(±)-**5**	Cl	51	165 ± 4	20.9	51.3	5.5
(±)-**6**	Br	81	471 ± 8	32.0	56.8	5.5
(±)-**7**	CN	356	289 ± 13	26.2	46.1	4.7
(±)-**8**	CF_3	665	330 ± 22	18.5	71.8	6.0

[a] Standard deviations are given. [b] Derived from the CSD searches in CSD 5.38 (February 2017). [c] Calculated with ACD/Percepta (GALAS prediction model) from ACD/Labs, release 2016.2.

ent, the energy difference between these two conformations is 2.4 kcal mol^{-1}, whereas it is calculated as 9.4 kcal mol^{-1} for the CF_3 derivative (±)-**8**.

It is likely that the substituent-dependent conformation of the biphenyl moiety influences the cell-based efficacy by affecting cell permeation. Cell permeation occurs by means of passive diffusion, carrier proteins (transporters), and channel proteins.[50,51] Passive diffusion is thought to be the main contributor to permeation and is less sensitive (or not sensitive at all) to the stereochemistry of a drug, whereas configuration and conformation matters with transporters.[50] Transporters are complex systems to study and in *P. falciparum* their number has not been clearly defined yet. Gardner et al. first reported a limited number of transporters, around 50.[52] Later, a bioinformatics analysis by Martin et al. revealed twice as many transporters.[53] Carrier proteins can be drug targets, but play also a role in resistance mechanism. Indeed, the *P. falciparum* chloroquine-resistant transporter (*Pf*CRT) is responsible for the resistance developed towards chloroquine.[54] Regarding our series of inhibitors (±)-**2**–**8**, it is conceivable that the biphenyl moiety needs to adopt a conformation close to co-planarity for the biphenyl to better penetrate into the cell. To our knowledge, such an effect of a torsion angle on cell-based efficacy has not been observed so far. Nonetheless, it is important to mention a study involving inhibitors of the ABCC2/MRP2 transporters, in which the affinity for the transporter was influenced by the conformation of a biphenyl moiety.[55] In this study, larger torsion angles led to improved inhibition.

Disparity in serum albumin binding across this series of ligands could be another explanation for the cell-based SAR. However, our assay was supplemented with only 0.5% of ALBUMAX® II and it is therefore rather unlikely that the discrepancies in efficacy arose from protein binding. Finally, it should be emphasized that cell permeation can be influenced by several factors, such as lipophilicity, and that the measured cellular efficacy is certainly not solely governed by the torsion angle of the biphenyl motif.

Crystal structure determination of *Pv*SHMT in complex with (±)-3, (±)-4, (±)-5, and (±)-7

*Pv*SHMT was crystallized from a ternary complex of *Pv*SHMT, glycine, and either (±)-**3**, (±)-**4**, (±)-**5**, or (±)-**7** by using the microbatch method. The co-crystals diffracted to 2.5, 2.4, 2.2, and 2.6 Å resolution, respectively, and belong to the *C*2 space group. The structures were solved by molecular replacement, using the coordinates of a chain A protomer of *Pv*SHMT (PDB ID code: 4OYT) as the template.[24] Despite using a racemic

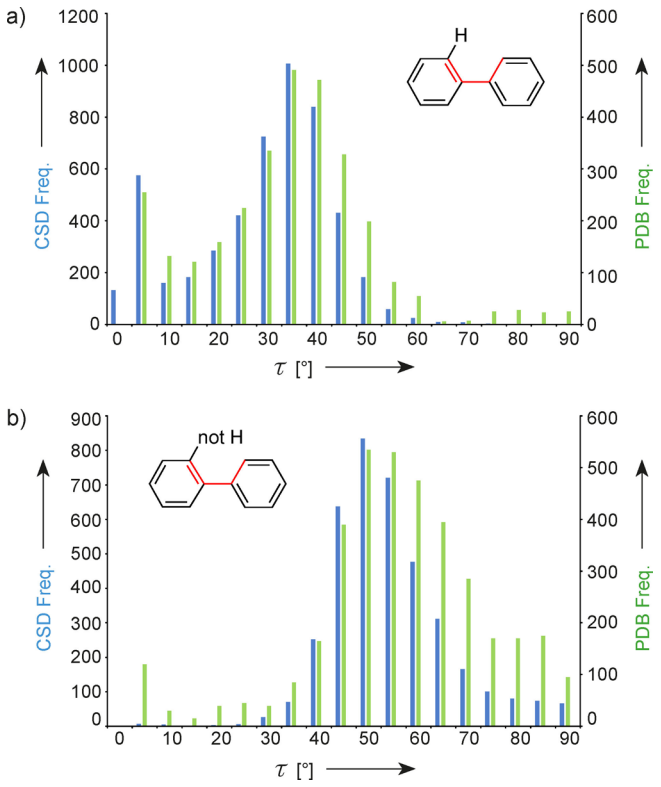

Figure 2. Torsion angle histograms derived from the CSD ligands (blue) and bound ligands in the PDB (green). a) Biphenyls without any *ortho*-substituent. b) *ortho*-Substituted biphenyls.

mixture of ligands for co-crystallization, only the (+)-(*S*) enantiomer was present in the structures. Importantly, both active sites of *Pv*SHMT were populated with a ligand in each complex (Supporting Information, Section S6.1.1, Figure S15).

Binding modes of (+)-3, (+)-4, (+)-5, and (+)-7

The pyrazolopyran core of (+)-**3**, (+)-**4**, (+)-**5**, and (+)-**7** occupies the pteridine binding pocket (Supporting Information, Section S6.1.1, Figure S16), as previously seen in other complexes with wild-type *Pv*SHMT.[25,26] It establishes an array of polar interactions, through the vinylogous cyanamide and the pyrazole ring, with key amino acids of *Pv*SHMT (Glu56, Leu124, Gly128, and Thr357). The measured torsion angles, ranging from 47° to 62° (Supporting Information, Section S6.1.1, Figure S17), are in good agreement with the CSD search (Table 1) and with the optimized structures (B3LYP/cc-pVDZ) (Supporting Information, Section S4, Figure S7). Although, it should be noted that the calculated structure of (+)-**5** exhibits a dihedral of 58°, which is markedly different than the 49° measured in the complex with *Pv*SHMT.

The main difference between those four co-crystal structures lies in the positioning of the *ortho*-substituent of the terminal phenyl ring (Figure 3). On the one hand, the halo ligands (+)-**3** and (+)-**5** adopt an anti-parallel alignment of their C–F/C–Cl bond dipole relative to the C–O dipole of Tyr63 (Figures 3a and 3c). The fluoride and chloride substituents in (+)-**3** and (+)-**5**, respectively, are in close proximity to Tyr63 and establish favorable local direct interactions[56–61] with the phenolic ring. On the other hand, the respective methyl and cyano moieties of (+)-**4** and (+)-**7** point towards Cys364 (Figures 3b and 3d). The torsion angle of (+)-**4** is equal to 62°, which sterically precludes the *ortho*-methyl group to lie below Tyr63. Indeed, with such torsion angle, the Me group would be at a sub-van der Waals distance to Tyr63. Instead of adopting a slightly different conformation to avoid a steric clash, ring flip occurs thereby enabling the Me group to interact with Leu124 and Cys364 (Figure 3b). Similarly, in order to avoid any repulsion of the C≡N moiety with the phenol ring of Tyr63, this substituent of (+)-**7** also points to Cys364 and lies almost orthogonally to one CH_3 group of Leu124 (Figure 3d). These structural distinctions, however, only have little impact onto target affinities (Table 1).

In the complexes with (+)-**4** and (+)-**5**, a water molecule (W1 or W2) solvating Tyr63 was resolved (Figures 3b and 3c). Additionally, W2 is in the vicinity of the chloroarene ring of (+)-**5** and establishes a weak O–H···π interaction.[62] Solvation of Tyr63 was also observed in a previous co-crystal structure of a pyrazolopyran-based ligand with *Pv*SHMT (PDB ID code: 5GVN).[26] Superimposition of the three co-crystal structures revealed a quasi-identical positioning of W1, W2, and W3 nearby Tyr63 (Supporting Information, Section S6.1.1, Figure S18).

Interestingly, in the second active site of the complex with (+)-**7** the cysteine bridge formed by Cys125 and Cys364 was found to be in its oxidized form (Supporting Information, Section S6.1.1, Figure S19). It is likely that the ligand bound to the active site in its reduced form and after a prolonged seeding period the disulfide bond was formed. Nevertheless, the binding mode of (+)-**7** remained identical to the one where the disulfide bridge is in its reduced form.

Aryl sulfonamide/aryl sulfone series

Sulfonamide motifs are widely used in chemical research, particularly in drug discovery, as illustrated with the antimalarial sulfadoxine,[63] and with the more recently approved drugs Asunaprevir (treatment of hepatitis C virus), Belinostat (antitumor agent), Glanatec® (treatment of glaucoma and ocular hypertension), or Vonoprazan fumarate (treatment of gastric ulcer).[64] As elegantly described by Kuhn et al., sulfonamides can be considered as "molecular chimeras, which are found to form hydrogen bonds as well as interact with unipolar environments within proteins".[8]

We were interested in improving the binding affinities in our class of inhibitors by harvesting favorable nonpolar contacts with residues such as Lys139, Val141, Ser263, and Pro267 at the exit of the *p*ABA channel (Supporting Information, Section S5, Figures S13 and S14). We implemented a sulfonamide group into a series of extended derivatives (±)-**9**–**17** to properly orient the terminal lipophilic moieties. In the modeling process, care was taken to consider the preferred orientation of aryl sulfonamide and aryl sulfone moieties. Previous studies showed that the sulfonamide conformation can markedly influence target affinity as in the development of factor Xa inhibi-

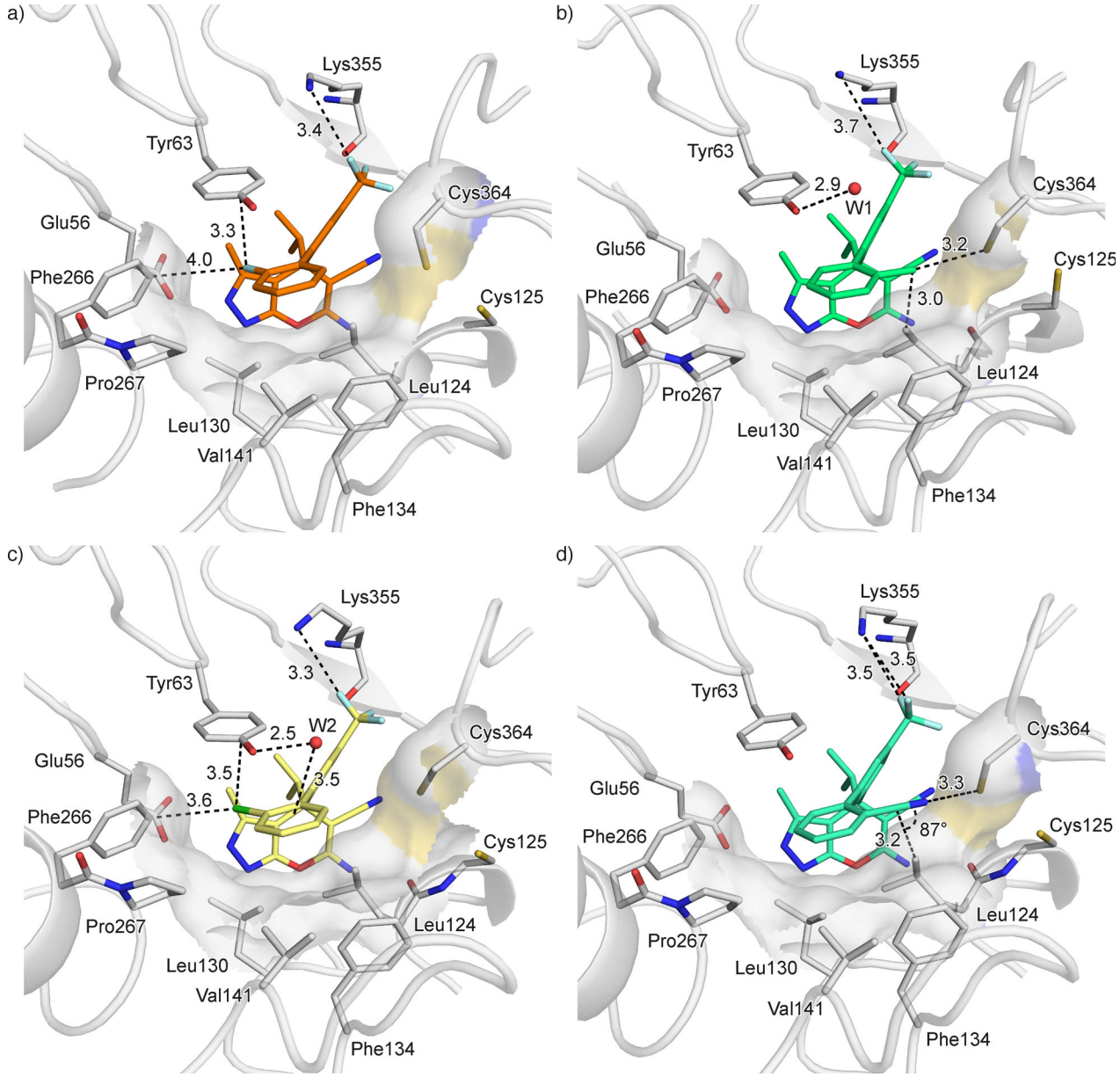

Figure 3. Co-crystal structures showing the protein-ligand interactions of *Pv*SHMT (grey) and pyrazolopyran ligands: a) (+)-**3** (orange; PDB ID code: 5XMS, 2.5 Å); b) (+)-**4** (lime; PDB ID code: 5XMU, 2.4 Å); c) (+)-**5** (gold; PDB ID code: 5XMV, 2.2 Å); d) (+)-**7** (cyan; PDB ID code: 5XMT, 2.6 Å). The surface spans the volume of the *p*ABA channel. Water molecules (W1 and W2) are represented as red spheres. PLP is omitted for clarity. Distances are given in Å. Color code: $C_{protein}$ grey, $C_{(+)\text{-}3}$ orange, $C_{(+)\text{-}4}$ lime, $C_{(+)\text{-}5}$ gold, $C_{(+)\text{-}7}$ cyan, Cl green, F light cyan, N blue, O red, S yellow.

tors.[38,39] There are two distinct dihedral angles in aryl sulfonamides and one in aryl sulfones that determine the conformational preferences of these fragments.

The first is the torsion angle about the C_{sp2}—S bond in both moieties. An extensive CSD search by Brameld et al. pinpointed the favored conformation of aryl sulfonamides and aryl sulfones, in which the π orbital of the *ipso*-carbon atom bisects the SO_2 angle,[7] a conformation described for the first time in 1986 by Beddoes et al. in an X-ray crystallographic analysis.[33] Since the number of structures deposited in the CSD increases exponentially over time, we performed a new search to update the results obtained by Brameld et al. (Figure 4a). In both motifs the torsion angles converge towards a maximum located around 90°, highlighting the conformation in which the π orbital of the *ipso*-carbon atom bisects the SO_2 angle. This favored conformation for aryl sulfonamides and aryl sulfones was also computed by density functional theory (DFT) (Figure 4b and Supporting Information, Section S4, Figure S10), which is in agreement with calculations performed in 2006.[37] Comparable results were obtained when searching in the PDB (Supporting Information, Section S3, Figure S2). However, a broader distribution was observed due to the lower accuracy in the determination of small-molecule conformation preferences in macromolecular X-ray structures, as several ligand poses can be fitted to electron densities.[65]

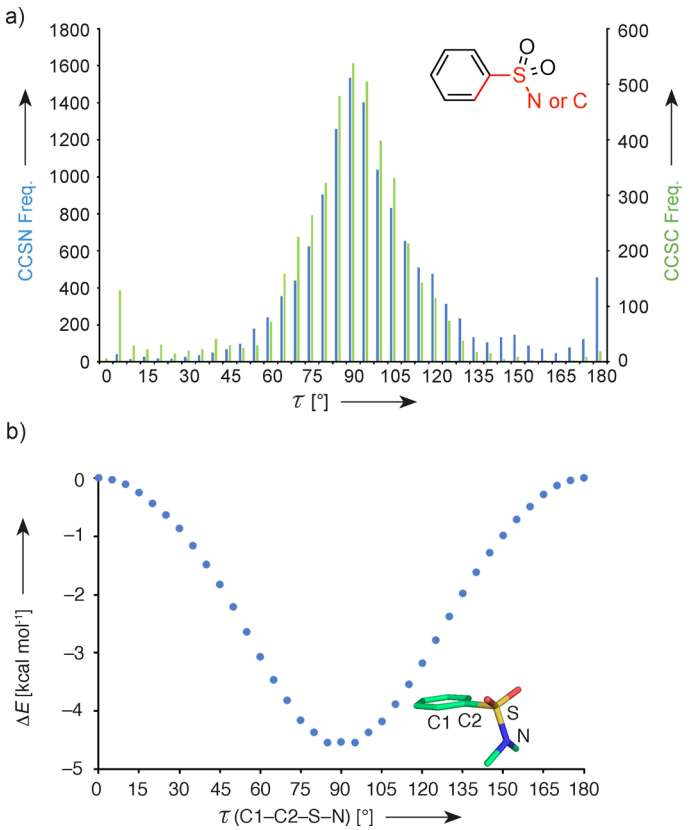

Figure 4. a) Torsion histogram derived from CSD ligands for aryl sulfonamides (blue) and aryl sulfones (green). b) Relative energy while driving the dihedral angle τ(C1-C2-S-N) of an aryl sulfonamide from 0–180°. DFT-B3LYP/cc-pVDZ calculations carried out in water (with polarizable continuum solvent model) using Gaussian 09.[49]

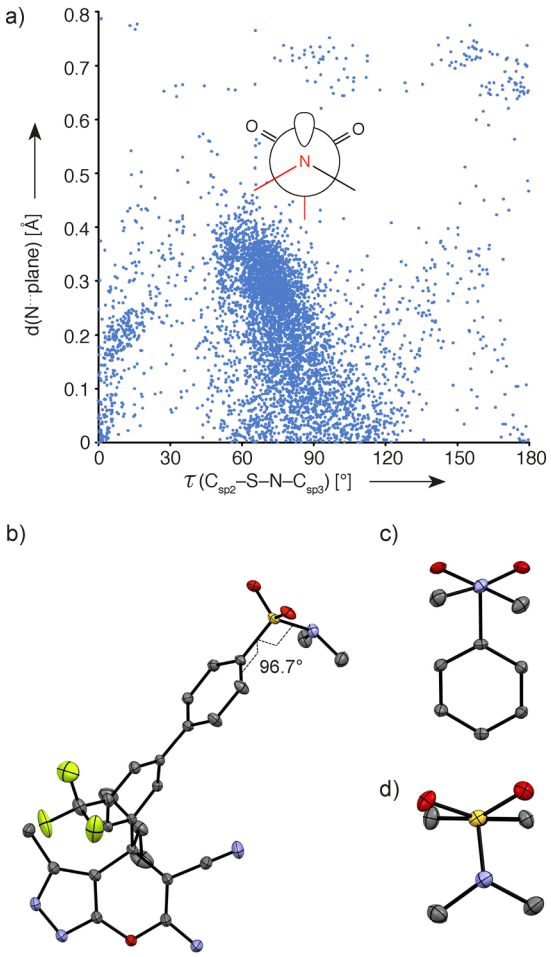

Figure 6. a) Scatterplot for *N*,*N*-disubstituted sulfonamides derived from the molecules in the CSD. The distance between N and the plane of its three substituents is plotted against the C_{sp2}-S-N-C_{sp3} torsion angle. The absolute value of the larger of the two alternative C_{sp2}-S-N-C_{sp3} torsion angles was chosen. b) ORTEP plot at the 50% probability level of the small-molecule crystal structure of (±)-**9** (for clarity hydrogen atoms are omitted and only (+)-**9** is shown). c) Front view of the sulfonamide from (+)-**9** showing the N-lone pair bisecting the O-S-O angle. d) Front view of the sulfonamide from (+)-**9** showing the π orbital of the *ipso*-carbon atom bisecting the O-S-O angle.

The second dihedral angle of interest in aryl sulfonamides is the C_{sp2}-S-N-C_{sp3} angle. This angle can adopt either an eclipsed or a staggered conformation (Figure 5). Early ab initio calculations on *N*-methylmethanesulfonamide predicted the eclipsed conformation to be the more stable with an energy barrier ranging from 1.46 kcal mol^{-1} (at the RHF/6-31G* level of theory)[34] to 2.63 kcal mol^{-1} (at the MP2/6-31G* level of theory).[35] Later, those results were contrasted by the crystal structure of *N*-methylmethanesulfonamide found in the staggered conformation only.[36]

In most of the molecules in the CSD and the PDB ligands, the C_{sp2}-S-N-C_{sp3} torsion angles are in a range between 60° and 90° meaning a clear preference for the staggered conformation with the nitrogen lone pair bisecting the SO_2 angle (Figure 6a and Supporting Information, Section S3, Figure S3). This conformational preference goes in parallel with decreased N-pyramidalization. The retrieved distances (<0.40 Å) between the nitrogen atom and the plane of its three substituents are characteristics of sulfonamides. The nitrogen atoms are generally slightly less pyramidal than in acyclic tertiary amines (d(N···plane) ≈ 0.45 Å).[7] In addition, PES at the B3LYP/cc-pVDZ and B3LYP/cc-pVTZ levels of theory (in water with polarizable continuum solvent model) for the fragments $PhSO_2NH_2$, $PhSO_2NHMe$, and $PhSO_2NMe_2$ (Supporting Information, Section S4, Figure S11), are in good agreement with the CSD and PDB searches. At both levels of theory, the staggered conformation was found to be favored over the eclipsed one. The preference for this conformation can be explained by stereoelectronic and steric effects. The nitrogen lone pair interacts in an antiperiplanar orientation with the σ* orbital of the weakest bond, which is the C_{sp2}–S bond. Steric repulsion might also

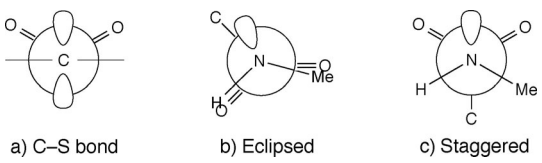

Figure 5. a) Stable conformation of aryl sulfonamides/aryl sulfones relative to the C_{sp2}–S bond. b) and c) Two energetically stable conformations of sulfonamides relative to the N–S bond.

favor the staggered over the eclipsed conformation, in particular if larger substituents are attached to the nitrogen atom.

The preference of the aryl sulfonamide moiety to adopt the staggered conformation is nicely illustrated by the small-molecule X-ray crystal structures recorded for (±)-**9**, (±)-**11**, and (±)-**16** (Figure 6b and Supporting Information, Sections S6.2.2, S6.2.3, and S6.2.4). The measured C_{sp2}-C_{sp2}-S-N torsion angles are equal to 96.7°, 90.9° and 79.9°, respectively, matching nicely the CSD search. In the three structures, the nitrogen lone pair perfectly bisects the SO_2 angle (Figure 6c and Supporting Information, Sections S6.2.2, S6.2.3, and S6.2.4).

A series of nine aryl sulfonamide analogues ((±)-**9**–**17**) was synthesized and tested on *Pf*- and *At*SHMT, as well as on the sensitive strain *Pf*NF54 (Table 2). All nitrogen substituents were selected based on MOLOC modeling to generate favorable interactions with the lipophilic residues at the exit of the *p*ABA channel. In the modeling, the more polar sulfonamide moiety in the staggered conformation was oriented towards the solvent. The outcome, however, was disappointing (Table 2). While the IC_{50} values against *At*SHMT were in the lower nanomolar range from 22.8 to 87.7 nM, a meaningful SAR was not recognizable (Table 2 and Supporting Information, Section S2, Table S1). Similarly, mixed results were obtained in the cell-based assay on *Pf*NF54 (Table 2). The biological activities suggested that no appreciable additional favorable contacts were harvested by the lipophilic nitrogen substituents. This was

Table 2. Biological activities of sulfonamides and sulfones (±)-**9**–**22**.

Cpd.	R	EC_{50} *Pf*NF54 [nM]	IC_{50} *At*SHMT [nM]	Cpd.	R	EC_{50} *Pf*NF54 [nM]	IC_{50} *At*SHMT [nM]
(±)-**9**	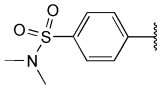	114	22.8	(±)-**17**	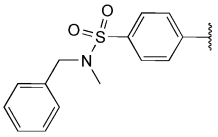	104	73.9
(±)-**10**	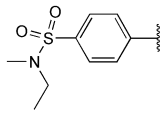	210	74.4	(+)-**17**		56	n.d.[a]
(±)-**11**	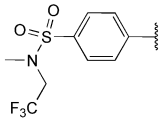	657	43.0	(−)-**17**		1584	n.d.
(±)-**12**	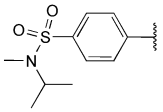	400	39.1	(±)-**18**	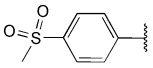	91	16.8
(±)-**13**	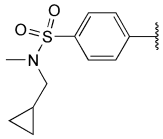	391	29.0	(±)-**19**	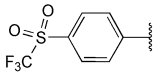	1399	n.d.
(±)-**14**	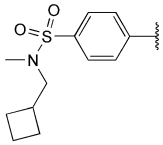	374	87.7	(±)-**20**	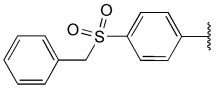	557	24.5
(±)-**15**	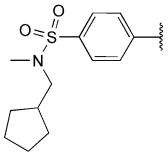	872	79.1	(±)-**21**		200	22.4
(±)-**16**	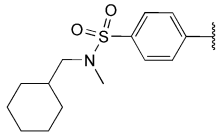	838	85.6	(±)-**22**		186	19.2

[a] n.d. = Not determined.

later confirmed by co-crystal structures analyses, as shown below.

The two enantiomers of the benzyl sulfonamide (±)-**17** were separated by chiral-phase HPLC to afford pure (+)-**17** and (−)-**17**. As already observed with other pyrazolopyran-based ligands,[25,26] there is a high level of chiral recognition at the active site of *Pf*SHMT and large discrepancies in biological activity were measured for (+)-**17** and (−)-**17**. Ligand (+)-**17** inhibited *Pf*SHMT (IC_{50} = 150 nM) much more efficiently than (−)-**17** (only 38% inhibition at 250 μM) (Supporting Information, Section S2, Table S1). The preference for the (+)-enantiomer is not surprising when considering the binding mode of pyrazolopyran-based ligands. Indeed, for all analogues co-crystallized with *Pv*SHMT in this program, exclusively the (+)-enantiomers were found to be bound to the enzyme. Cell-based efficacy confirmed this trend, as (+)-**17** was again much more potent than (−)-**17** (EC_{50} = 56 and 1584 nM, respectively) (Table 2).

Three ligands containing an aryl sulfone moiety ((±)-**18**–**20**) and two reverse sulfonamides ((±)-**21** and (±)-**22**) were also prepared, yielding target- and cell-based activities in a similar range to the aryl sulfonamide ligands (Table 2 and Supporting Information, Section S2, Table S1). Crystals of the reverse sulfonamide (±)-**21** also featured a staggered conformation with a C_{sp3}-N-S-C_{sp3} torsion angle of −71.8° (Supporting Information, Section 6.2.5, Figure S32). This moiety is twisted almost orthogonally with respect to the phenyl ring with a C_{sp2}-C_{sp2}-N-S torsion angle of 77.6° (Supporting Information, Section 6.2.5, Figure S31).

Although several ligands of both biphenyl and aryl sulfonamide/aryl sulfone series proved to be highly potent in our in vitro assays, they were not studied further due to their limited metabolic stability in human liver microsomes ($t_{1/2}$ < 10 min) (Supporting Information, Section S2, Table S2). The terminal fragments on the phenyl ring departing from the core are presumably responsible for this intrinsic instability and not the pyrazolopyran core. Indeed, we recently reported a series of pyrazolopyran-based ligands with half-lives up to 4 h.[26]

Crystal structure determination of C364A-*Pv*SHMT in complex with (±)-11, (±)-17, and (±)-20

Several attempts made to co-crystallize either (±)-**11**, (±)-**17**, or (±)-**20** with wild-type *Pv*SHMT showed no electron density of the bound ligands. Instead, a partial or full formation of the disulfide bridge between Cys125 and Cys364 was observed. To circumvent the cysteine oxidation and prevent the disulfide bridge formation, which might be linked to the binding of the ligands, Cys364 was mutated to Ala364. Subsequently, co-crystal structures of (+)-**11**, (+)-**17**, or (+)-**20** with the C364A-*Pv*SHMT mutant were obtained. The co-crystals diffracted to 2.4, 2.2, and 2.6 Å resolution, respectively, and belong to the *C*2 space group. The structures were solved by molecular replacement using the coordinates of a chain A protomer of *Pv*SHMT (PDB ID code: 4OYT) as the template.[24] Despite using a racemic mixture of ligands for co-crystallization, only the (+)-(*S*) enantiomer was present in all structures. In the three protein–ligand complexes, both active sites were found populated by a ligand (Supporting Information, Section 6.1.2, Figure S20).

Binding mode of (+)-11, (+)-17, and (+)-20

Gratifyingly, the three co-crystal structures provided an explanation for the lacking additional gain in affinity by the lipophilic residues at the termini of the aryl sulfonamides and aryl sulfones.

The binding mode of the pyrazolopyran core was found to be the same as in all other co-crystals with wild-type *Pv*SHMT solved so far, with a strong hydrogen-bonding network anchoring this scaffold into the pteridine binding pocket (Figure 7a and Supporting Information, Section S6.1.2, Figures S21a and S22a). The sulfonamide moieties in (+)-**11** and (+)-**17** and the sulfone in (+)-**20** are nicely found in their favored conformation with C_{sp2}-C_{sp2}-S-N (or C_{sp2}-C_{sp2}-S-C_{sp3}) torsion angles of 74°, 86°, and 98°, respectively. However, the orientation of the sulfonamide moiety in (+)-**11** (Supporting Information, Section S6.1.2, Figure S21b) and (+)-**17** (Figure 7b), and the sulfone moiety in (+)-**20** (Supporting Information, Section S6.1.2, Figure S22b) was found to be opposite to that predicted by modeling (Supporting Information, Section S5, Figures S13 and S14). The SO_2 moiety is pointing towards the hydrophobic residues at the exit of the *p*ABA channel, while the hydrophobic terminal substituents of the ligands are all pointing towards solvent instead of interacting with the protein. Indeed, the sulfonamide moiety of (+)-**17** is at close distances to Val141 (d(O···H–C_{Val141}) = 2.8 and 3.3 Å) and Pro267 (d(O···H–C_{Pro267}) = 3.2 Å), establishing several van der Waals interactions with apolar atoms and forming weak hydrogen-bond-type contacts to aliphatic C–H moieties (Figure 7b).[41] Very similar interactions were found for (+)-**11** and (+)-**20** with contacts ranging from 2.8 to 3.4 Å (Supporting Information, Section S6.1.2, Figures S21b and S22b). Those three C364A-*Pv*SHMT–ligand complexes highlight the low hydrophilicity of the SO_2 group, which resembles the low hydrophilicity of the nitro group[66] that also prefers pointing into hydrophobic pockets rather than into solvent. We performed a search in both CSD and PDB for hydrogen bonding from strong hydrogen-bond donors (O–H and N–H, but excluding C–H) to the SO_2 group in aryl sulfonamides and aryl sulfones (Supporting Information, Section S3, Table S3). Of 7856 hits in the CSD, 6617 sulfonamides formed no hydrogen bond and 1239 one hydrogen bond. A higher frequency of single hydrogen bonds was retrieved from the PDB, as 847 out of 1410 hits formed one hydrogen bond. Cases of two hydrogen bonds were rarer in both the CSD and PDB, with 37 and 496 hits, respectively. Regarding structures containing a sulfone moiety, only 344 hits out of the 2352 in the CSD established one hydrogen bond, and approximately half of the hits in the PDB. Only a limited number of sulfone formed two hydrogen bonds (Supporting Information, Section S3, Table S3). The distances of the hydrogen bonds to the SO_2 group are in a range of 2.8 to 3.5 Å (Supporting Information, Section S3, Figure S4) and no specific directionality was observed as the hydrogen bonds cover the

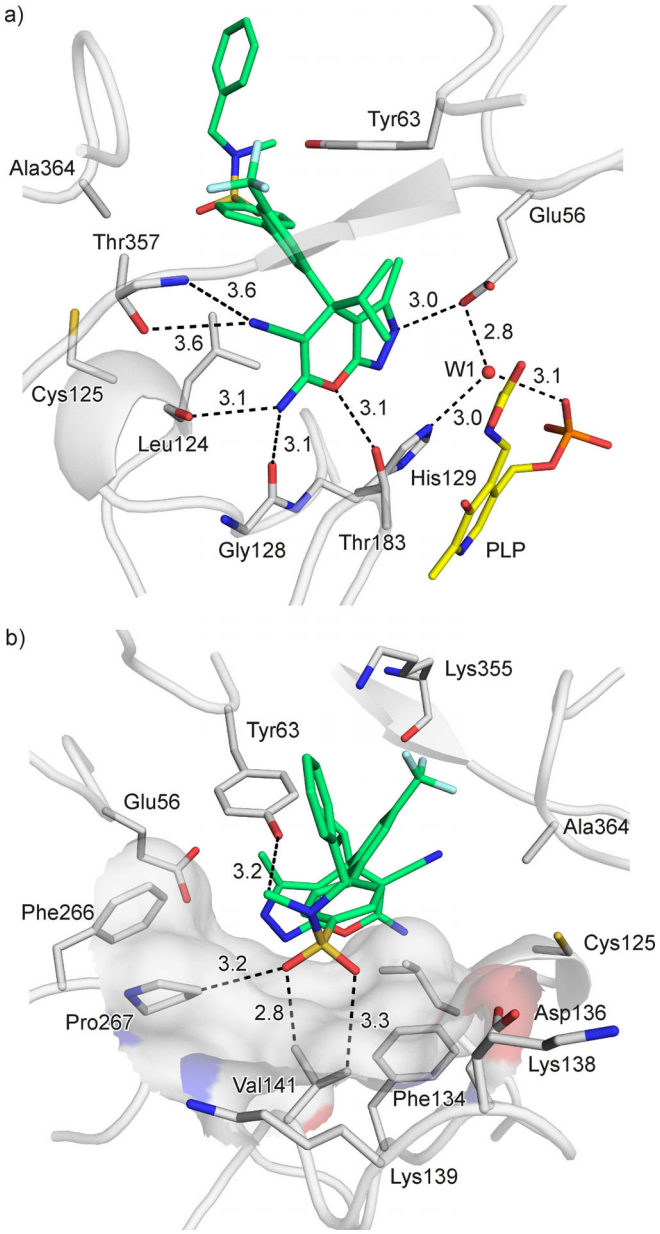

Figure 7. Co-crystal structure (PDB ID code: 5XMQ, 2.2 Å) showing the protein–ligand interactions of pyrazolopyran (+)-**17** (lime) and C364A-*Pv*SHMT mutant (grey). a) Polar interactions between (+)-**17** and the protein. b) Interactions, largely dipole-dipole type, involving the sulfonamide moiety in the *p*ABA channel. The surface spans the volume of the *p*ABA channel. The water molecule (W1) is represented as a red sphere. PLP is omitted for clarity in b). Distances are given in Å. Color code: $C_{protein}$ grey, $C_{(+)\text{-}17}$ lime, C_{PLP} gold, F light cyan, N blue, O red, P orange, S yellow.

hemisphere around one of the S=O bonds (Supporting Information, Section S3, Figures S5 and S6).

Conclusions

Based on X-ray co-crystal structures information, two series of SHMT inhibitors featuring widely used chemical motifs, namely biphenyl and aryl sulfonamide/aryl sulfone moieties, were synthesized, and tested on targets *At*- and *Pf*SHMT, and in vitro on the *Pf*NF54 strain. The aim of this study was to introduce lipophilic moieties on pyrazolopyran-based ligands to improve their affinities by enhancing the lipophilic contacts with the *p*ABA channel of the enzyme.

Regarding the seven biphenyl analogues ((±)-**2**–**8**), similar target affinities across the series were measured on *At*SHMT and *Pf*SHMT. However, the cell-based potency of those compounds was dramatically impacted by the nature of the *ortho*-substituent with differences in EC_{50} values up to 37-fold. To explain these results, we performed CSD and PDB searches, as well as a potential energy scan (PES) of the considered biphenyls. We found that the loss of cellular efficacy correlates with the increase of the torsion angle of the biphenyl, which depends on the size of its *ortho*-substituent. We postulate that cell permeation was impacted by the conformational changes of the biphenyls and this was accounted for the disparity between the efficacies on *Pf*NF54. A total of four *Pv*SHMT–ligand co-crystal structures were solved for this series of molecules. Interestingly, in the complexes with (+)-**3** and (+)-**5** the *ortho*-halo substituent is turned towards Tyr63, undergoing antiparallel dipolar C–X···C–O interactions with the C–O bond of Tyr63 and local direct electrostatic interactions with the aromatic ring. In contrast, in the co-crystal structures with (+)-**4** and (+)-**7**, their respective methyl and cyano substituents point to Cys364 to avoid steric repulsion with Tyr63.

In parallel, fourteen ligands bearing an aryl sulfonamide or an aryl sulfone moiety ((±)-**9**–**22**) were examined. By CSD and PDB searches, as well as by theoretical calculations, we demonstrated that aryl sulfonamides and aryl sulfones preferentially adopt a conformation in which the π orbital of the *ipso*-carbon atom bisects the O-S-O angle.[7] We also showed the preference for the nitrogen lone pair of sulfonamides to bisect the O-S-O angle, resulting in a characteristic staggered conformation. Small-molecule X-ray crystal structures of pyrazolopyran-based inhibitors nicely illustrated these favored conformations. No significant activity gain was measured, regardless of the size of the terminal apolar moiety grafted onto the sulfonamide/sulfone. This could be rationalized with the help of three co-crystal structures of (+)-**11**, (+)-**17**, and (+)-**20** with a C364A-*Pv*SHMT mutant, in which the respective sulfonyl moieties were found pointing towards the hydrophobic residues lining the *p*ABA channel and establishing several short van der Waals interactions. That way, the terminal apolar groups grafted onto the sulfonamide point into the bulk and cannot interact with the protein to improve the binding affinity. These co-crystal structures, complemented by CSD and PDB searches, highlight the low hydrophilicity of the SO_2 moiety, which prefers to point to hydrophobic environments rather than into polar ones. Effective chiral recognition at the active site was shown, with the target binding of enantiopure ligand (+)-**17** being largely preferred over (−)-**17**. Taken together, this investigation provided valuable input, not only regarding the development of SHMT inhibitors, but also for the general design of drug-like molecules that incorporate the discussed functional groups.

Experimental Section

Chemical synthesis: All synthetic protocols and analytical data of the preparation of ligands (±)-**2**–**22** and their respective intermediates are detailed in the Supporting Information, Sections S1, S7, and S8.

In vitro antimalarial activity: The *Plasmodium falciparum* drug-sensitive NF54 strain was cultivated in a variation of the medium previously described, consisting of RPMI 1640 supplemented with 0.5% ALBUMAX® II, 25 mM Hepes, 25 mM $NaHCO_3$ buffer (pH 7.3), 0.36 mM hypoxanthine, and 100 μg mL^{-1} neomycin.[67,68] Human erythrocytes served as host cells. Cultures were maintained in an atmosphere of 3% O_2, 4% CO_2, and 93% N_2 in modular chambers at 37 °C. Compounds were dissolved in DMSO (10 mg mL^{-1}), diluted in hypoxanthine-free culture medium, and titrated in duplicates over a 64-fold range in 96 well plates. Infected erythrocytes (1.25% final hematocrit and 0.3% final parasitemia) were added into the wells. After 48 h incubation, 0.25 μCi of [^{3}H]hypoxanthine was added and plates were incubated for an additional 24 h. Parasites were harvested onto glass-fiber filters, and radioactivity was counted using a MicroBeta2 plate liquid scintillation counter (PerkinElmer). The results were recorded and expressed as a percentage of the untreated controls. Fifty percent effective concentrations (EC_{50}) were estimated by linear interpolation.[69]

Enzymatic *Pf*SHMT assay: Assay reactions (200 μL total volume) contained SHMT (≈0.5 μM), L-serine (2 mM), (6*S*)-H_4F (0.4 mM), β-$NADP^+$ (0.25 mM), and the coupling enzyme methylene tetrahydrofolate dehydrogenase (FolD, 5 μM) in 50 mM HEPES pH 7.0 containing 1 mM DTT and 0.5 mM EDTA. To this mixture, inhibitors (1 μL) with various concentrations were added and initial rates of the reaction monitored to measure the activity of the enzyme. The inhibitors were dissolved in DMSO, and the control assays without inhibitor but in the presence of 0.5% DMSO (final concentration) were also carried out.

Enzymatic *At*SHMT assay: Assay reactions (200 μL total volume) contained SHMT (1 μg), L-serine (20 mM), (6*S*)-H_4F (0.3 mM), β-NAD^+ (2 mM) and the coupling enzyme methylene tetrahydrofolate dehydrogenase (FolD, 20 μg) in 50 mM potassium phosphate buffer pH 7.4, containing 7.5 mM DTT. To this mixture inhibitors (10 μL) with various concentrations (final concentrations from 1–1000 nM) were added and initial rates of the reaction monitored to measure the amount of non-inhibited enzyme. The inhibitors were dissolved in 80% DMSO, and the control assays without inhibitor in the presence of 1% DMSO (final concentration) were also carried out. The accumulation of NADH was followed for 20 minutes at 340 nm using a BioTek Synergy HTX plate reader.

Crystallization of recombinant *Pv*SHMT and compounds (±)-3, (±)-4, (±)-5, (±)-7, (±)-11, (±)-17, and (±)-20: *Pv*SHMT (or C364A-*Pv*SHMT) was crystallized using a microbatch method in a 60-well plate (Ø 1 mm at bottom of each well) covered with baby oil (6 mL; Johnson; a mixture of mineral oil, olive oil, and vitamin E, PZ Johnson, Thailand). Protein–ligand complexes were prepared by mixing purified *Pv*SHMT protein (60 μL; 20–25 mg mL^{-1}) with 1 mM PLP, 60 mM β-mercaptoethanol, 90 mM of glycine, and 5.7 mM (±)-**3**, or (±)-**4**, or (±)-**5**, or (±)-**7**, or (±)-**11**, or (±)-**17**, or (±)-**20**. The mixture was equilibrated on ice for 30 min to allow complete complex formation. The crystallization drop was composed of 1 μL each of a crystallization solution and the protein complex. Protein crystals of *Pv*SHMT were grown at 293 K in 20–24% w/v PEG4000, 0.06–0.12 M NaCl, 0.1 M Tris-HCl buffer pH 8.5.

***Pv*SHMT crystal structure data collection, structure determination and refinement:** A single crystal was flash-vitrified in liquid nitrogen using 20% glycerol in crystallizing agent as a cryoprotectant. X-ray diffraction data were collected at 100 K at wavelength of 1 Å using ADSC Quantum-315 CCD detector at beamline 13B1, NSRRC (Taiwan). Data were processed using the HKL2000 package. X-ray diffraction data and refinement statistics are listed in Supporting Information, Section S6.1.1, Table S4 and Section S6.1.2, Table S5. The structure of *Pv*SHMT (or C364A-*Pv*SHMT) was determined by molecular replacement using *Phaser* in CCP4 suite with a chain A protomer of *Pv*SHMT coordinate (PDB ID code: 4OYT) as the template. Model building and structure refinement were carried out using *Coot* and *Refmac5*. The ligand structure was prepared using *HYPERCHEM*.

Acknowledgements

Work at ETH Zurich was supported by a grant from the ETH Research Council (ETH-01 13-2). At ETH Zurich, we thank Dr. Bruno Bernet for help with the compound characterizations and Michael Solar for recording the small-molecule X-ray structures. We thank the MMV foundation, especially Dr. Jeremy Burrows and Dr. Roger Bonnert, for their support, for giving us access to their assay network, and their great expertise. We also acknowledge Dr. Karen White and Dr. Susan Charman at CDCO for performing microsomal stability assays. We are grateful to Abhijit Kundu and Surajit Sadhukhan at TCG Lifesciences for providing free-of-charge several key building blocks for the synthesis. Protein–ligand studies including *Plasmodium* enzyme inhibition and protein crystallography were financially supported by grants from Cluster Program and Management Office, National Science and Technology development Agency, Thailand (CPMO-P-13-00835), National Center for Genetic Engineering and Biotechnology (Platform P-14-50241), the Thailand Research Fund (RTA5980001), and Mahidol University. We gratefully acknowledge the National Synchrotron Radiation Research Center (Taiwan) for the beamline 13B1 and the operating staff. We thank the experimental facility and the technical services provided by the "Synchrotron Radiation Protein Crystallography Facility of the National Core Facility Program for Biotechnology, Ministry of Science and Technology" and the "National Synchrotron Radiation Research Center", a national user facility supported by the Ministry of Science and Technology, Taiwan, ROC.

Conflict of interest

The authors declare no conflict of interest.

Keywords: co-crystal structures · conformation analysis · drug design · plasmodium · serine hydroxymethyltransferase

[1] J. A. Feng, I. Aliagas, P. Bergeron, J. M. Blaney, E. K. Bradley, M. F. T. Koehler, M.-L. Lee, D. F. Ortwine, V. Tsui, J. Wu, A. Gobbi, *J. Comput.-Aided Mol. Des.* **2015**, *29*, 511 – 523.
[2] A. Hillisch, N. Heinrich, H. Wild, *ChemMedChem* **2015**, *10*, 1958 – 1962.
[3] B. Kuhn, M. Tichý, L. Wang, S. Robinson, R. E. Martin, A. Kuglstatter, J. Benz, M. Giroud, T. Schirmeister, R. Abel, F. Diederich, J. Hert, *J. Med. Chem.* **2017**, *60*, 2485 – 2497.

[4] C. Lerner, A. Ruf, V. Gramlich, B. Masjost, G. Zürcher, R. Jakob-Roetne, E. Borroni, F. Diederich, *Angew. Chem. Int. Ed.* **2001**, *40*, 4040 – 4042; *Angew. Chem.* **2001**, *113*, 4164 – 4166.
[5] M. Giroud, J. Ivkovic, M. Martignoni, M. Fleuti, N. Trapp, W. Haap, A. Kuglstatter, J. Benz, B. Kuhn, T. Schirmeister, F. Diederich, *ChemMedChem* **2017**, *12*, 257 – 270.
[6] J. Boström, P.-O. Norrby, T. Liljefors, *J. Comput.-Aided Mol. Des.* **1998**, *12*, 383 – 396.
[7] K. A. Brameld, B. Kuhn, D. C. Reuter, M. Stahl, *J. Chem. Inf. Model.* **2008**, *48*, 1 – 24.
[8] B. Kuhn, W. Guba, J. Hert, D. Banner, C. Bissantz, S. Ceccarelli, W. Haap, M. Körner, A. Kuglstatter, C. Lerner, P. Mattei, W. Neidhart, E. Pinard, M. G. Rudolph, T. Schulz-Gasch, T. Woltering, M. Stahl, *J. Med. Chem.* **2016**, *59*, 4087 – 4102.
[9] B. M. Hudson, E. Nguyen, D. J. Tantillo, *Org. Biomol. Chem.* **2016**, *14*, 3975 – 3980.
[10] I.-J. Chen, N. Foloppe, *Drug Dev. Res.* **2011**, *72*, 85 – 94.
[11] R. Taylor, *Acta Crystallogr. Sect. D* **2002**, *58*, 879 – 888.
[12] F. H. Allen, R. Taylor, *Chem. Soc. Rev.* **2004**, *33*, 463 – 475.
[13] G. M. Battle, G. M. Ferrence, F. H. Allen, *J. Appl. Crystallogr.* **2010**, *43*, 1208 – 1223.
[14] E. Pidcock, J. A. Chisholm, P. A. Wood, P. T. A. Galek, L. Fábián, O. Korb, A. J. Cruz-Cabeza, J. W. Liebeschuetz, C. R. Groom, F. H. Allen in *Supramolecular Chemistry: From Molecules to Nanomaterials Vol. 6* (Eds. J. W. Steed, P. A. Gale), Wiley, Chichester, **2012**, pp. 2927 – 2946.
[15] CCDC Website database, Accessed April 25, **2017**. http://www.ccdc.cam.ac.uk/solutions/csd-system/components/csd/
[16] C. R. Groom, F. H. Allen, *Angew. Chem. Int. Ed.* **2014**, *53*, 662 – 671; *Angew. Chem.* **2014**, *126*, 675 – 684.
[17] S. J. Cottrell, T. S. G. Olsson, R. Taylor, J. C. Cole, J. W. Liebeschuetz, *J. Chem. Inf. Model.* **2012**, *52*, 956 – 962.
[18] J. E. Salcedo-Sora, S. A. Ward, *Mol. Biochem. Parasitol.* **2013**, *188*, 51 – 62.
[19] I. B. Müller, J. E. Hyde, *Mol. Biochem. Parasitol.* **2013**, *188*, 63 – 77.
[20] V. Schirch, D. M. E. Szebenyi, *Curr. Opin. Chem. Biol.* **2005**, *9*, 482 – 487.
[21] S. Maenpuen, K. Sopitthummakhun, Y. Yuthavong, P. Chaiyen, U. Leartsakulpanich, *Mol. Biochem. Parasitol.* **2009**, *168*, 63 – 73.
[22] C. K. T. Pang, J. H. Hunter, R. Gujjar, R. Podutoori, J. Bowman, D. G. Mudeppa, P. K. Rathod, *Mol. Biochem. Parasitol.* **2009**, *168*, 74 – 83.
[23] P. Chitnumsub, W. Ittarat, A. Jaruwat, K. Noytanom, W. Amornwatcharapong, W. Pornthanakasem, P. Chaiyen, Y. Yuthavong, U. Leartsakulpanich, *Acta Crystallogr. Sect. D* **2014**, *70*, 1517 – 1527.
[24] P. Chitnumsub, A. Jaruwat, P. Riangrungroj, W. Ittarat, K. Noytanom, W. Oonanant, J. Vanichthanankul, P. Chuankhayan, S. Maenpuen, C.-J. Chen, P. Chaiyen, Y. Yuthavong, U. Leartsakulpanich, *Acta Crystallogr. Sect. D* **2014**, *70*, 3177 – 3186.
[25] M. C. Witschel, M. Rottmann, A. Schwab, U. Leartsakulpanich, P. Chitnumsub, M. Seet, S. Tonazzi, G. Schwertz, F. Stelzer, T. Mietzner, C. McNamara, F. Thater, C. Freymond, A. Jaruwat, C. Pinthong, P. Riangrungroj, M. Oufir, M. Hamburger, P. Mäser, L. M. Sanz-Alonso, S. Charman, S. Wittlin, Y. Yuthavong, P. Chaiyen, F. Diederich, *J. Med. Chem.* **2015**, *58*, 3117 – 3130.
[26] G. Schwertz, M. C. Witschel, M. Rottmann, R. Bonnert, U. Leartsakulpanich, P. Chitnumsub, A. Jaruwat, W. Ittarat, A. Schäfer, R. A. Aponte, S. A. Charman, K. L. White, A. Kundu, S. Sadhukhan, M. Lloyd, G. M. Freiberg, M. Srikumaran, M. Siggel, A. Zwyssig, P. Chaiyen, F. Diederich, *J. Med. Chem.* **2017**, *60*, 4840 – 4860.
[27] H. M. Berman, J. Westbrook, Z. Feng, G. Gilliland, T. N. Bhat, H. Weissig, I. N. Shindyalov, P. E. Bourne, *Nucleic Acids Res.* **2000**, *28*, 235 – 242.
[28] H. Berman, K. Henrick, H. Nakamura, *Nat. Struct. Biol.* **2003**, *10*, 980.
[29] E. L. Eliel, S. H. Wilen, L. N. Mander in *Stereochemistry of Organic Compounds*, Wiley, New York, **1994**, pp. 1142 – 1155.
[30] D. Vonlanthen, A. Mishchenko, M. Elbing, M. Neuburger, T. Wandlowski, M. Mayor, *Angew. Chem. Int. Ed.* **2009**, *48*, 8886 – 8890; *Angew. Chem.* **2009**, *121*, 9048 – 9052.
[31] E. Masson, *Org. Biomol. Chem.* **2013**, *11*, 2859 – 2871.
[32] While several earlier papers provided evidence for the distinct conformational preferences of aryl sulfonamides and aryl sulfones, they were brought to the attention to the broader medicinal and organic chemistry communities by Dr. Klaus Müller (F. Hoffman-La Roche), in seminar series worldwide, such as at ETH Zurich in 2004.
[33] R. L. Beddoes, L. Dalton, J. A. Joule, O. S. Mills, J. D. Street, C. I. F. Watt, *J. Chem. Soc. Perkin Trans. 2* **1986**, 787 – 797.
[34] J. B. Nicholas, R. Vance, E. Martin, B. J. Burke, A. J. Hopfinger, *J. Phys. Chem.* **1991**, *95*, 9803 – 9811.
[35] G. Liang, J. P. Bays, J. P. Bowen, *J. Mol. Struct.: THEOCHEM* **1997**, *401*, 165 – 179.
[36] T. C. Higgs, A. Parkin, S. Parsons, P. A. Tasker, *Acta Crystallogr. Sect. E* **2002**, *58*, o523 – o525.
[37] F. Hof, A. Schütz, C. Fäh, S. Meyer, D. Bur, J. Liu, D. E. Goldberg, F. Diederich, *Angew. Chem. Int. Ed.* **2006**, *45*, 2138 – 2141; *Angew. Chem.* **2006**, *118*, 2193 – 2196.
[38] S. Senger, M. A. Convery, C. Chan, N. S. Watson, *Bioorg. Med. Chem. Lett.* **2006**, *16*, 5731 – 5735.
[39] S. Senger, C. Chan, M. A. Convery, J. A. Hubbard, G. P. Shah, N. S. Watson, R. J. Young, *Bioorg. Med. Chem. Lett.* **2007**, *17*, 2931 – 2934.
[40] A. K. H. Hirsch, M. S. Alphey, S. Lauw, M. Seet, L. Barandun, W. Eisenreich, F. Rohdich, W. N. Hunter, A. Bacher, F. Diederich, *Org. Biomol. Chem.* **2008**, *6*, 2719 – 2730.
[41] C. Bissantz, B. Kuhn, M. Stahl, *J. Med. Chem.* **2010**, *53*, 5061 – 5084.
[42] P. R. Gerber, K. Müller, *J. Comput.-Aided Mol. Des.* **1995**, *9*, 251 – 268.
[43] S. Kotha, K. Lahari, D. Kashinath, *Tetrahedron* **2002**, *58*, 9633 – 9695.
[44] A. R. Muci, S. L. Buchwald, *Top. Curr. Chem.* **2002**, *219*, 131 – 209.
[45] G. Jones, *Org. React.* **1967**, *15*, 204 – 599.
[46] M. Witschel, F. Stelzer, J. Hutzler, T. Qu, T. Mietzner, K. Kreuz, K. Grossmann, R. Aponte, H. W. Höffken, F. Calo, T. Ehrhardt, A. Simon, L. Parra Rapado, WO 2013/182472 A1, **2013**.
[47] CSD search: CSD version 5.38, February 2017, containing about 875 000 entries. All searches were performed with ConQuest 1.19 for structures with *R*-factor $< 10\%$ (no error, no partial disorder), excluding polymeric, powder, or metalorganic compounds. PDB search: Searches were performed using Relibase + v3.2.0. All searches were limited to resolution of protein crystal structures ≤ 2.5 Å.
[48] C. P. Brock, R. P. Minton, *J. Am. Chem. Soc.* **1989**, *111*, 4586 – 4593.
[49] Gaussian 09, Revision A.02, M. J. Frisch, G. W. Trucks, H. B. Schlegel, G. E. Scuseria, M. A. Robb, J. R. Cheeseman, G. Scalmani, V. Barone, G. A. Petersson, H. Nakatsuji, M. Caricato, A. Marenich, J. Bloino, B. G. Janesko, R. Gomperts, B. Menucci, H. P. Hratchian, J. V. Ortiz, A. F. Izmaylov, J. L. Sonnenberg, D. Williams-Young, F. Ding, F. Lipparini, F. Egidi, J. Goings, B. Peng, A. Petrone, T. Henderson, D. Ranasinghe, V. G. Zakrzewski, J. Gao, N. Rega, G. Zheng, W. Liang, M. Hada, M. Ehara, K. Toyota, R. Fukuda, J. Hasegawa, M. Ishida, T. Nakajima, Y. Honda, O. Kitao, H. Nakai, T. Vreven, K. Throssell, J. A. Montgomery, Jr., J. E. Peralta, F. Ogliaro, M. Bearpark, J. J. Heyd, E. Brothers, K. N. Kudin, V. N. Staroverov, T. Keith, R. Kobayashi, J. Normand, K. Raghavachari, A. Rendell, J. C. Burant, S. S. Iyengar, J. Tomasi, M. Cossi, J. M. Millam, M. Klene, C. Adamo, R. Cammi, J. W. Ochterski, R. L. Martin, K. Morokuma, Ö. Farkas, J. B. Foresman, D. J. Fox, Gaussian, Inc., Wallingford CT, **2016**.
[50] K. Sugano, M. Kansy, P. Artursson, A. Avdeef, S. Bendels, L. Di, G. F. Ecker, B. Faller, H. Fischer, G. Gerebtzoff, H. Lennernaes, F. Senner, *Nat. Rev. Drug Discovery* **2010**, *9*, 597 – 614.
[51] N. Noinaj, S. K. Buchanan, *Curr. Opin. Struct. Biol.* **2014**, *27*, 8 – 15.
[52] M. J. Gardner, et. al., *Nature* **2002**, *419*, 498 – 511.
[53] R. E. Martin, R. I. Henry, J. L. Abbey, J. D. Clements, K. Kirk, *Genome Biol.* **2005**, *6*, R26.
[54] A. Ecker, A. M. Lehane, J. Clain, D. A. Fidock, *Trends Parasitol.* **2012**, *28*, 504 – 514.
[55] Y. Lai, L. Xing, G. I. Poda, Y. Hu, *Drug Metab. Dispos.* **2007**, *35*, 937 – 945.
[56] S. E. Wheeler, K. N. Houk, *J. Am. Chem. Soc.* **2008**, *130*, 10854 – 10855.
[57] S. E. Wheeler, *J. Am. Chem. Soc.* **2011**, *133*, 10262 – 10274.
[58] S. E. Wheeler, *Acc. Chem. Res.* **2013**, *46*, 1029 – 1038.
[59] R. M. Parrish, C. D. Sherrill, *J. Am. Chem. Soc.* **2014**, *136*, 17386 – 17389.
[60] M. Harder, M. A. Carnero Corrales, N. Trapp, B. Kuhn, F. Diederich, *Chem. Eur. J.* **2015**, *21*, 8455 – 8463.
[61] L.-J. Riwar, N. Trapp, B. Kuhn, F. Diederich, *Angew. Chem. Int. Ed.* **2017**, *56*, 11252 – 11257; *Angew. Chem.* **2017**, *129*, 11405 – 11410.
[62] L. M. Salonen, M. Ellermann, F. Diederich, *Angew. Chem. Int. Ed.* **2011**, *50*, 4808 – 4842; *Angew. Chem.* **2011**, *123*, 4908 – 4944.
[63] A. Nzila, *J. Antimicrob. Chemother.* **2006**, *57*, 1043 – 1054.
[64] A. C. Flick, H. X. Ding, C. A. Leverett, R. E. Kyne, Jr., K. K.-C. Liu, S. J. Fink, C. J. O'Donnell, *Bioorg. Med. Chem.* **2016**, *24*, 1937 – 1980.

[65] G. L. Warren, T. D. Do, B. P. Kelley, A. Nicholls, S. D. Warren, *Drug Discovery Today* **2012**, *17*, 1270 – 1281.
[66] N. Sagawa, T. Shikata, *Phys. Chem. Chem. Phys.* **2014**, *16*, 13262 – 13270.
[67] A. Dorn, R. Stoffel, H. Matile, A. Bubendorf, R. G. Ridley, *Nature* **1995**, *374*, 269 – 271.
[68] W. Trager, J. B. Jensen, *Science* **1976**, *193*, 673 – 675.
[69] W. Huber, J. C. Koella, *Acta Tropica* **1993**, *55*, 257 – 261.

Manuscript received: July 13, 2017
Revised manuscript received: August 15, 2017
Version of record online: ■■ ▮▮, 0000

FULL PAPER

Drug Design

*G. Schwertz, M. S. Frei, M. C. Witschel, M. Rottmann, U. Leartsakulpanich, P. Chitnumsub, A. Jaruwat, W. Ittarat, A. Schäfer, R. A. Aponte, N. Trapp, K. Mark, P. Chaiyen, F. Diederich**

■■ – ■■

Conformational Aspects in the Design of Inhibitors for Serine Hydroxymethyltransferase (SHMT): Biphenyl, Aryl Sulfonamide, and Aryl Sulfone Motifs

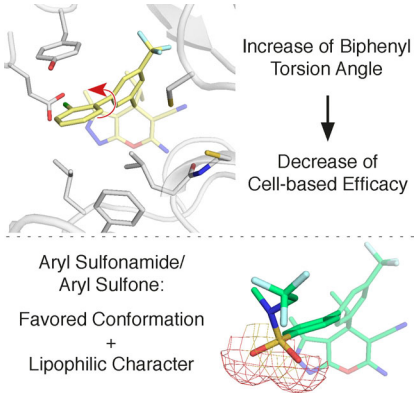

Mind the conformation! Two potent series of pyrazolopyran-based inhibitors of the enzyme serine hydroxymethyltransferase (SHMT), bearing either terminal biphenyl, aryl sulfonamide, or aryl sulfone motif are reported. The substantial influence of the torsion angle of the biphenyl moiety on the cell-based efficacy is discussed. Additionally, the preferred conformations of aryl sulfonamide/aryl sulfone moieties and their lipophilic character in the complexes with *P. vivax* SHMT were analyzed.